

Variable Quasi Periodic Oscillations during an outburst of the transient X-ray pulsar XTE J1858+034

U. Mukherjee¹, S. Bapna², H. Raichur^{1,3}, B. Paul¹, S. N. A. Jaaffrey³

¹Tata Institute of Fundamental Research,
Homi Bhabha Road, Colaba, Mumbai 400005

²Department of Physics, College of Science,
M. L. Sukhadia University, Rajasthan 313001, India

³Joint Astronomy Program, Indian Institute of Science, Bangalore-560 012

Abstract.

We have investigated the Quasi Periodic Oscillation (QPO) properties of the transient accreting X-ray pulsar XTE J1858+034 during the second outburst of this source in April-May 2004. We have used observations made with the Proportional Counter Array (PCA) of the Rossi X-ray Timing Explorer (RXTE) during May 14-18 2004, in the declining phase of the outburst. We detected the presence of low frequency QPOs in the frequency range of 140–185 mHz in all the RXTE-PCA observations. We report evolution of the QPO parameters with the time, X-ray flux, and X-ray photon energy. Though a correlation between the QPO centroid frequency and the instantaneous X-ray flux is not very clear from the data, we point out that the QPO frequency and the one day averaged X-ray flux decreased with time during these observations. We have obtained a clear energy dependence of the RMS variation in the QPOs, increasing from about 3% at 3 keV to 6% at 25 keV. The X-ray pulse profile is a single peaked sinusoidal, with pulse fraction increasing from 20% at 3 keV to 45% at 30 keV. We found that, similar to the previous outburst, the energy spectrum is well fitted with a model consisting of a cut-off power law along with an iron emission line.

keywords stars: pulsar: individual (XTE J1858+034) — X-rays:pulsar

1. Introduction

Among the accretion powered X-ray pulsars, Quasi Periodic Oscillations (QPO) were first discovered in the X-ray flux of the transient source EXO 2030+375 (Angelini et al. 1989). Since then, QPOs have been detected in the X-ray power density spectra of almost a dozen accretion-powered pulsars (Psaltis 2004). QPO centre frequencies as seen in the pulsars vary widely, ranging from 1 mHz to 40 Hz. In the models that deal with QPOs in X-ray pulsars, a correlation is expected between the QPO centre and the X-ray flux, which in turn is determined by the mass accretion rate. Hence, intensity dependent variable QPOs can provide an interesting insight into the physics of accretion. However, QPOs are in general rare and transient events in X-ray pulsars.

To date, six out of the dozen X-ray Binary Pulsars (XBP) showing QPOs are transient sources (Psaltis 2004). XTE J1858+034 is one of the transient XBPs in which QPOs have been detected. This X-ray binary was discovered with the RXTE All Sky Monitor (ASM) in 1998 February during a transient outburst (Remillard & Levine 1998). Observations made with the Proportional Counter Array (PCA) of the RXTE during the first outburst of the source showed single peaked strong sinusoidal pulsations with a period of ~ 221.0 s (Takeshima et al. 1998, Paul & Rao 1998). QPOs at 110 mHz with about 7% RMS fluctuation were discovered from the same observation (Paul & Rao 1998). The energy spectrum was measured to be hard, similar to the spectra of XBPs. From the transient nature of this source, its hard X-ray spectrum, and presence of pulsations, it was suggested to be a Be-X-ray binary (Takeshima et al. 1998) which is also supported from the optical observations of H_α emission line (Reig, Kougentakis & Papamastorakis 2004).

The source had a second outburst that was first detected with INTEGRAL in March 2004 and subsequently again in April, 2004 (Molkov et al. 2004). The RXTE-ASM also detected the outburst and it was followed up with the RXTE-PCA. We detected the QPO features again during this second outburst from an observation made on May 14, 2004. Subsequently, a series of target of opportunity observation of XTE J1858+034 were made with RXTE during May 16–18 to study the evolution of the QPO properties. We have investigated the evolution of the QPO parameters with time, X-ray flux and X-ray photon energy. X-ray pulsation properties and the X-ray spectrum were also measured from these observations. In the following sections we present the X-ray observations, analysis and results and a discussion based on the results obtained.

2. Observations

The observations of XTE J1858+034 reported here were made during May 14–18, 2004 with the pointed mode instruments of the RXTE satellite. The

RXTE-ASM lightcurve of XTE J1858+034 is shown in Figure 1 for the period of March-May 2004 with a bin-size of one and a half days. The ASM light curve clearly shows that during the RXTE pointed observations, the source was in the decaying phase of this outburst.

The RXTE satellite carries a large area Proportional Counter Array (PCA), consisting of five Xenon filled proportional counter units (PCUs) sensitive in the energy range of 2–60 keV with a total effective area of 6250 cm² (Jahoda et al. 1996). It also has a set of high energy crystal scintillation experiment (HEXTE; 15–200 keV; 1600 cm² area), and a continuously scanning all-sky monitor (ASM; 2–10 keV; 90 cm²). A full description of the ASM detector can be found in Bradt et al. (1993). Here we have used the RXTE-ASM long term light curve of XTE J1858+034 available from the beginning of the RXTE mission in 1995 to the present and data from six pointed observations with RXTE-PCA. The details of the observations used in the present work have been given in a nutshell in Table 1. In total there were data from eight orbits of the satellite. Two of the six observations, Obs. B & F had two orbits of data each (B1, B2 & F1, F2 in Table 1). The total good time interval (GTI) with the PCA from these six observations was 18.7 ks. Figure 1 shows the RXTE-ASM long term light curve (bin size of one and a half days for clarity) along with the background subtracted RXTE-PCA count rates superposed on it. Though the beginning of the outburst is not clear, the gradual fall in the long term intensity can be clearly seen from the figure.

3. Data Analysis and Results

3.1 Light curve & Pulse Profile

From all the eight segments in the six observations, we extracted the light curves, each with a bin size of 0.125 s and then applied Barycentre correction on them. All the individual light curves showed the pulses. The combined background subtracted light curve of all the six observations binned at the pulse period of ~ 220 s had an average count rate of ~ 260 counts s⁻¹ and also had a gradual fall in intensity with time (see figure 2). The pulse folding and the χ^2 maximization method gave a pulse period of 219.823 ± 0.005 s within 90% confidence interval. A slow transient pulsar is expected to have a large spin-up rate in a high intensity state like this. However, a small duty cycle during the five days of observation does not allow us to measure the spin-up rate. The 2-60 keV X-ray light curve, obtained from the PCA detectors is shown in Figure 2. This figure is generated with a binsize of 220 s, same as the spin period, which removes the pulsation related intensity variations. Though the overall intensity changed with time, there was no significant intensity variation at a time scale of a few thousand seconds.

We have folded the energy resolved background subtracted light curves

with the pulse period mentioned above and the resultant pulse profiles are shown in Figure 3 for observation A. The pulse profiles shown for six out of the eight energy bands are single peaked sinusoidal in energy bands up to 25-35 keV range with a pulse fraction (defined as Maximum-Minimum/Maximum) gradually increasing from 20% at 3 keV to 45% at 30 keV. From Figure 3, we see that pulsations exist upto 45 keV also with a pulse fraction of 35% in the energy band of 35-45 keV. Pulsations above 45 keV is not detectable with the PCA due to low signal to noise ratio and low detection efficiency.

3.2 *Power density spectrum & related results*

We have generated the Power Density Spectra (PDS) from the 2-60 keV 0.125 s time resolved light curves from each orbit of the satellite. The light curves were broken into segments of length 128 s and the PDS obtained from each of these segments were averaged to produce the final PDS for data from each orbit of the satellite. A broad QPO feature between 100 mHz and 200 mHz was very prominent in all the PDS. The continuum of the PDS in the frequency range of 7 mHz to 2 Hz fits well with a model consisting of a power law. The prominent QPO feature is fitted well with a Gaussian model component. In most of the PDS, there is also an evidence for a second QPO peak, probably a harmonic of the fundamental. However, we have refrained from quantifying the second peak as it has very low statistics. In Figure 4 we have shown the power density spectrum from observation C which has a power-law index of -0.93 and the Gaussian, QPO feature centered at 160 mHz. Evolution of the QPO frequency and the associated RMS for the eight data segments are shown in Figure 5. While the QPO frequency decreased with time from 185 mHz on May 14th to about 140 mHz on May 18th, the RMS variability associated with the QPO did not have any significant change. The RMS variability in the QPO feature is of the order of 4.0 % to 3.0 %. In order to investigate the energy dependence of the QPO feature, we generated PDS in the five energy bands of 2-5 keV, 5-8 keV, 8-12 keV, 12-18 keV and 18-30 keV respectively for Obs A. We did not find any evidence of a QPO beyond the 18-30 keV band though. The PDS in the different energy bands were more or less identical in shape, and were fitted with the same model as described above. The RMS variation in the QPO feature in different X-ray energy bands obtained from observation A is plotted in Figure 6. We have obtained a clear energy dependence of the RMS variation in the QPOs, increasing from about 3% at 3 keV to 6% at 25 keV. The QPO centroid frequency is plotted against the 3-30 keV RXTE-PCA flux in Figure 7, which does not show a clear correlation between the two.

3.3 Energy spectrum

For spectral analysis, we used the Standard-2 dataset from PCA which is stored with 16 s time resolution. We first extracted the source plus background spectra from all the eight segments of observation. The background spectra were modeled using the “**pcabackest**” package provided by the XTE guest observer facility (GOF). On the average three PCUs were ON, and data from all the PCUs were added together to produce the spectrum. Channels corresponding to energy less than 3 keV and greater than 30 keV were ignored because of low signal to noise ratio. Although the background simulation model that we have used takes care of the internal background, emission from an extended source like the Galactic ridge or the cosmic X-ray background are not included in it. From a detailed observation of the Galactic ridge obtained using the PCAs (Valinia & Marshall 1998), we have estimated that about 1.0 % of the observed flux can be accounted for by the Galactic ridge emission and a very small fraction by the cosmic X-ray background. We have, therefore, explicitly incorporated the Galactic ridge emission as a sum of Raymond-Smith plasma and a power-law with appropriate normalizations. For fitting the pulse-phase averaged X-ray spectrum of the X-ray we have used a high energy cut-off power law along with a Gaussian emission line. The pulsar spectrum in the 3–30 keV range is found to be very hard with a photon index ~ 1.5 , cut-off energy of ~ 17 keV and e-folding energy of ~ 16 keV along with a neutral absorption with a equivalent Hydrogen column density of $\sim 10^{23}$ atoms cm^{-2} . The spectrum did not show any significant variation over the five days of observations. During these observations, the X-ray flux in the 3–30 keV range varied between 2.9×10^{-9} to 5.5×10^{-9} erg cm^{-2} s^{-1} . The X-ray spectrum from one of the observations is shown in figure 7 along with the best fit model and the residuals.

4. Discussion

QPOs in accretion powered X-ray pulsars are in general explained with either the beat frequency model or the Keplerian frequency model. In the former (Alpar & Shaham 1985), blobs of matter orbit the Neutron Star (NS) at approximately the Keplerian orbital frequency of the inner edge of the accretion disk. The magnetic field rotates at the frequency of the NS and material inflow to the NS is modulated at the Keplerian frequency. If ν_k is the Keplerian frequency of the inner edge of the disk and ν_s be the spin frequency of the NS, then according to the beat frequency model, the frequency of the QPO (ν_{QPO}) is given by the relation $\nu_{QPO} = \nu_k - \nu_s$. According to the latter model (Van der Klis et al. 1987), the inner edge of the accretion disk contains structures that modulate the observed flux by obscuration and gives rise to a QPO at ν_k . A third model by Shirakawa & Lai (2002) is known as the magnetic disk precession model. It attributes the presence of

QPOs in XBPs to the magnetically driven disk warping/precession, concentrated near the inner edge of the disk, at the magnetospheric boundary. The warping and precession of the disk arises from the magnetic torques which are present due to the interactions between the stellar field and the induced electric currents in the disk.

Out of the six transient XBPs showing QPOs, luminosity dependent QPO properties have been studied extensively for the two sources EXO 2030+375 (Angelini et al. 1989) and 3A 0535+262 (Finger, Wilson & Harmon 1996) and both the beat and Keplerian frequency models are applicable to a good extent. In several XBPs with QPOs like Her X-1, Cen X-3, 4U 1626-67, LMC X-4 and SMC X-1, and two transients V 0332+52 and 4U 0115+63, the QPO frequency is lower than the pulsation frequency (Psaltis 2004). In these sources, the Keplerian frequency model is not applicable, since a Keplerian rotation frequency of the inner accretion disk that is smaller than the spin frequency of the neutron star will result into centrifugal inhibition of accretion. Again, for V 0332+52, the beat frequency model may also not be viable since the value of the magnetospheric boundary calculated from the QPO properties and from the observed luminosity do not agree (Takeshima et al. 1994). In the Low Mass XBP GRO J1744-28, both these models are eliminated since in this source also $\nu_{QPO} < \nu_s$ and a flux change by a factor of ~ 7.5 did not have any corresponding change in QPO frequency.

The magnetic disk precession model (Shirakawa & Lai 2002) can explain the very low frequency QPOs in the XBPs, like in 4U 1626-67 (1 mHz) and may also explain the lowest frequency QPOs detected in some of the other XBPs (Her X-1, LMC X-4, and 4U 0115+63). While this model robustly accounts for QPOs with frequencies of the order of 1 mHz, the QPO frequency of XTE J1858+034 is two orders of magnitude higher and in this model, the production of QPOs at higher frequency depends on the details of the physics at the inner edge of the disk. Applicability of the magnetic disk precession model is therefore uncertain in this source.

It has already been mentioned that both the beat frequency and the Keplerian frequency models of QPOs predict a systematic increase of QPO frequency with the mass-accretion rate, which can be investigated by looking at the change of QPO frequency with the X-ray flux. This assumption is generally applicable to transient XBPs, in which the relation between X-ray luminosity and spin-up torque is well understood. The spin-up torque is in turn related to the mass accretion rate, inner radius of the accretion disk and rotation frequency of the inner disk. As the transient XBPs experience a wide range of mass-accretion rates, these are ideal objects to understand the QPO phenomena. In the case of XTE J1858+034 during the present outburst, we have detected changes in the QPO frequency over a span of five days. There is no discernible correlation between the QPO frequency and the instantaneous X-ray flux measured from the PCA data,

at least during the observation duration (Figure 7). However, as seen from the RXTE-ASM lightcurve, there is a gradual decrease in the overall one and a half day averaged X-ray intensity and a gradual decrease in the QPO frequency (from 185 mHz to 140 mHz, Figure 5) is also present during these observations. It may be possible that there is a correlation between the QPO frequency with the overall X-ray intensity or mass accretion rate which is not reflected in the short term. We note that in the RXTE-PCA observations of XTE J1858+034 made during the 1998 outburst, the source had a count rate (normalised for per detector unit) which was about a factor of 2.5–3.0 times less compared to the observations reported here. A smaller QPO frequency of 110 mHz during the 1998 outburst (Paul & Rao 1998) compared to the 140–185 mHz frequency during the 2004 outburst supports an inner accretion disk origin of the QPOs.

Absorption of X-rays by structures in the accretion disk should not be effective in producing hard X-ray QPOs and this process should definitely be more effective at lower X-ray energy. The detection of QPOs upto an energy of 30 keV and energy dependence of the RMS variability of the QPOs (Figure 6) shows that the Keplerian frequency model is unlikely to be applicable in the case of XTE J1858+034. Considering the strong energy dependence of the QPO rms detected both during the 1998 and the 2004 outbursts, and the possibility of a correlation between the QPO frequency with the overall X-ray intensity as discussed above, the beat frequency model seems to be more suitable in the case of XTE J1858+034.

Spectral parameters of XTE J1858+034 obtained from the RXTE-PCA observations during the second outburst in 2004 are similar to those measured during the previous outburst (Paul & Rao 1998). The iron emission line has an equivalent width in the range of 125 eV to 200 eV and the line centre energy is in the range of 6.3–6.7 keV. With the moderate resolution spectral data from the RXTE-PCA detectors we cannot conclude about the emission line characteristics, but it is likely that the emission line is from neutral or lowly ionized iron in the circumstellar material. The column density measured during the present observations is in the range of $(7.7 - 12.3) \times 10^{22}$ atoms cm^{-2} , which is higher than the same during the previous outburst. As the absorption column density depends on the mass loss history of the companion star prior to the outburst, a change in the column density is quite likely. We note that the iron line equivalent width and the absorption column density is consistent with a scenario in which the iron line is produced in a spherical shell of material which also causes the low energy X-ray absorption.

Acknowledgements

This research has made use of data obtained from the High Energy Astrophysics Science Archive Research Center (HEASARC), provided by NASA's Goddard Space Flight Center. UM and HR would like to acknowledge the Kanwal Rekhi Scholarship of TIFR Endowment Fund for partial financial support. We also thank Parag Shah for his help in system administration.

References

- Alpar, M., A., and J., Shaham, 1985, *Nature*, **316**, 239
 Angelini, L., Stella, L., & Parmar, A., N., 1989, *ApJ*, **346**, 906
 Bradt, H., V., Rothschild, R., E., & Swank, J., H., 1993, *A&AS*, **97**, 355
 Finger, M., H., Wilson, R., B., & Harmon, B., A., 1996, *ApJ*, **459**, 288
 Jahoda, K., Swank, J., H., Giles, A., B., et.al., 1996, in: Siegmund O.H.W., Gummin M.A. (eds.) EUV, X-Ray and Gamma-Ray Instrumentation for Astronomy VII. **SPIE 2808**, p. **59**
 Molkov, S., V. et al., 2004, *ATel*, **274**, 1M
 Paul, B., and Rao, A., R., 1998, *A&A*, **337**, 815
 Psaltis, D., **astro-ph/0410536**
 Remillard, R., and Levine, A., 1998, *IAUC 6826*
 Reig, P., Kougentakis, T., & Papamastorakis, G., 2004, *ATel*, **308**
 Shirakawa, A., & Lai, D., 2002, *ApJ*, **565**, 1134
 Takeshima, T., Dotani, T., Mitsuda, K., & Nagase, F., 1994, *ApJ*, **436**, 871
 Takeshima, T., Corbet, R., H., D., Marshall, F., E., Swank, J., H., & Chakrabarty, D., 1998, *IAUC 6826*
 Valinia, A., and Marshall, F., E., 1998, *ApJ*, **505**, 134
 Van der Klis et al., 1987, *ApJ*, **313**, **L19**

Table 1. Observation Log

Observations	Date	Start Time (UT)	Stop Time (UT)	Exposure (s)	Count Rate (s ⁻¹)
A	2004-05-14	11:30	12:26	3344	365
B1	2004-05-16	11:14	11:42	1665	422
B2	2004-05-16	13:54	14:48	3213	428
C	2004-05-16	18:47	19:21	2017	399
D	2004-05-16	20:24	20:45	1225	408
E	2004-05-16	23:41	00:05	1403	331
F1	2004-05-18	13:11	14:06	3297	279
F2	2004-05-18	14:43	15:25	2517	277

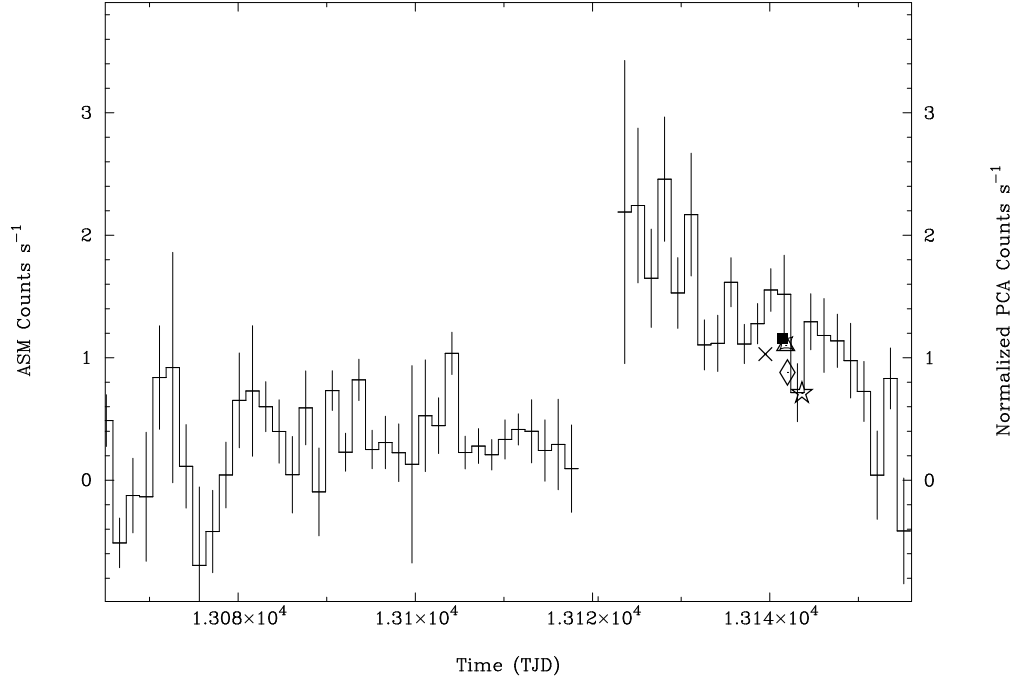


Figure 1. The section of the RXTE-ASM long term light curve depicted between March 1 to May 31, 2005, showing the 2004 outburst in detail. The bin size is one and a half days. The six PCA observations are shown (with different markers) with their respective background subtracted count rates (normalized by the mean count rate).

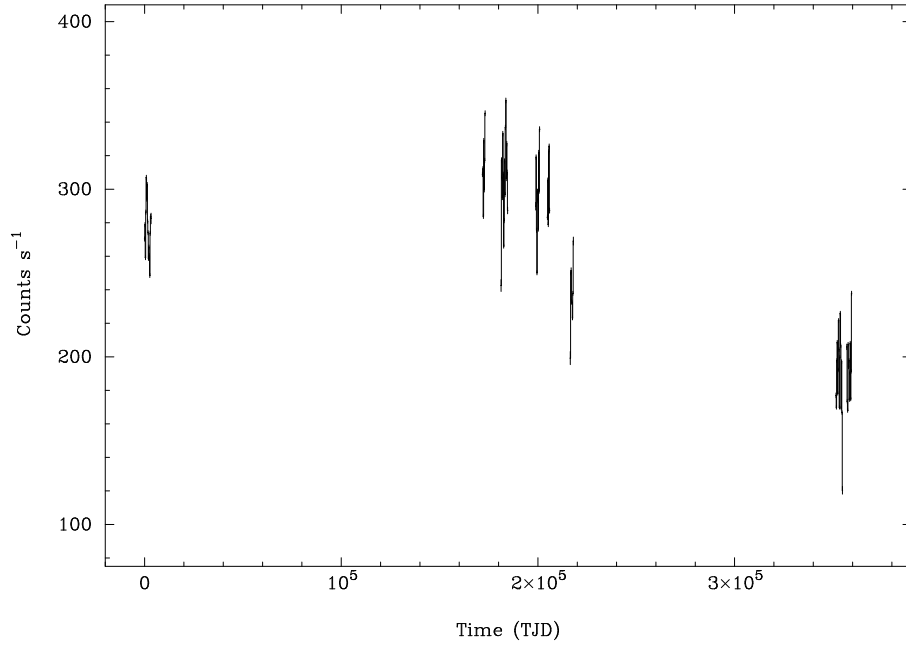


Figure 2. The RXTE-PCA background subtracted light curve in the energy band of 2-60 keV obtained from the 2004 observations is shown here with a binsize of 220 s.

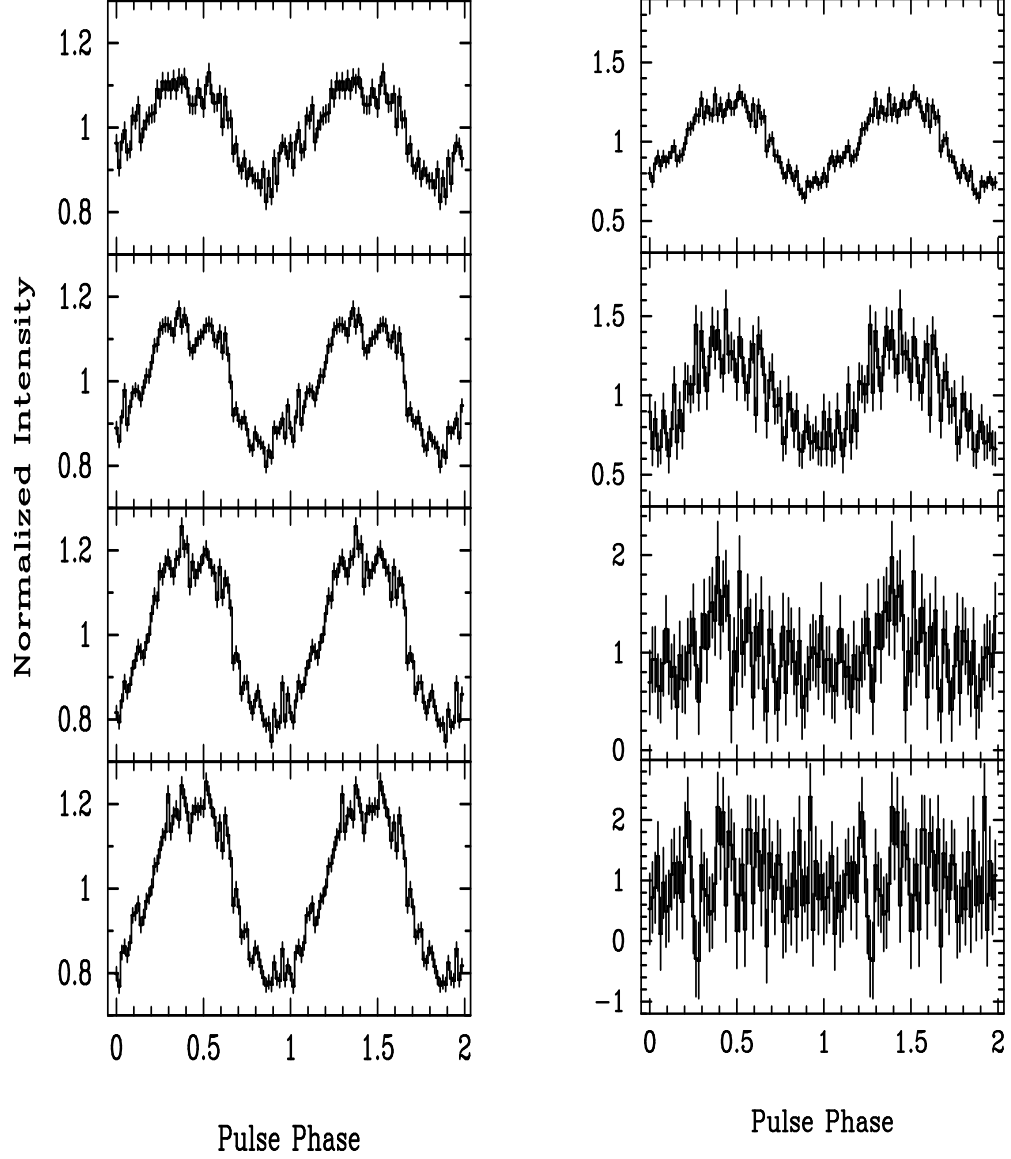


Figure 3. The nearly sinusoidal pulse profiles of XTE J1858+034 folded at a period of 219.8 s are shown (left, from the top) for 2-5 keV (first panel), 5-8 keV (second panel), 8-12 keV (third panel) and 12-18 keV (fourth panel). In the right the same is shown for 18-25 keV (top panel), 25-35 keV (second panel), 35-45 keV (third panel) and 45-60 keV (bottom panel) energy bands. The bottom-right panel shows that pulsations are not detectable with the PCA above 45 keV.

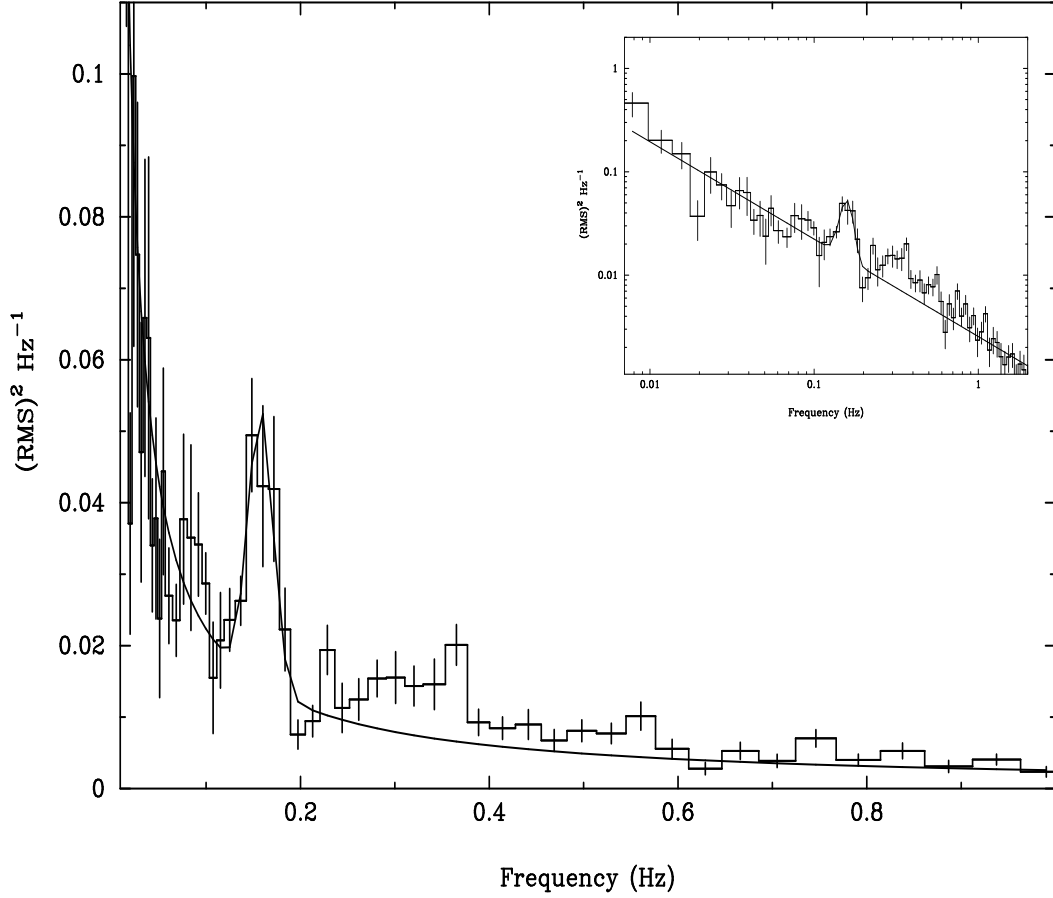


Figure 4. The power density spectrum of XTE J1858+034 generated from the 0.125 s binned lightcurve of Obs. C over the entire energy band of the PCA (in linear scale). The line represents the best fitted model in the frequency range of 0.007–2.0 Hz (shown for a restricted range to highlight the QPO feature) consisting of a power law and a Gaussian centred at the QPO frequency. The figure in the inset is a log-log plot of the same fit.

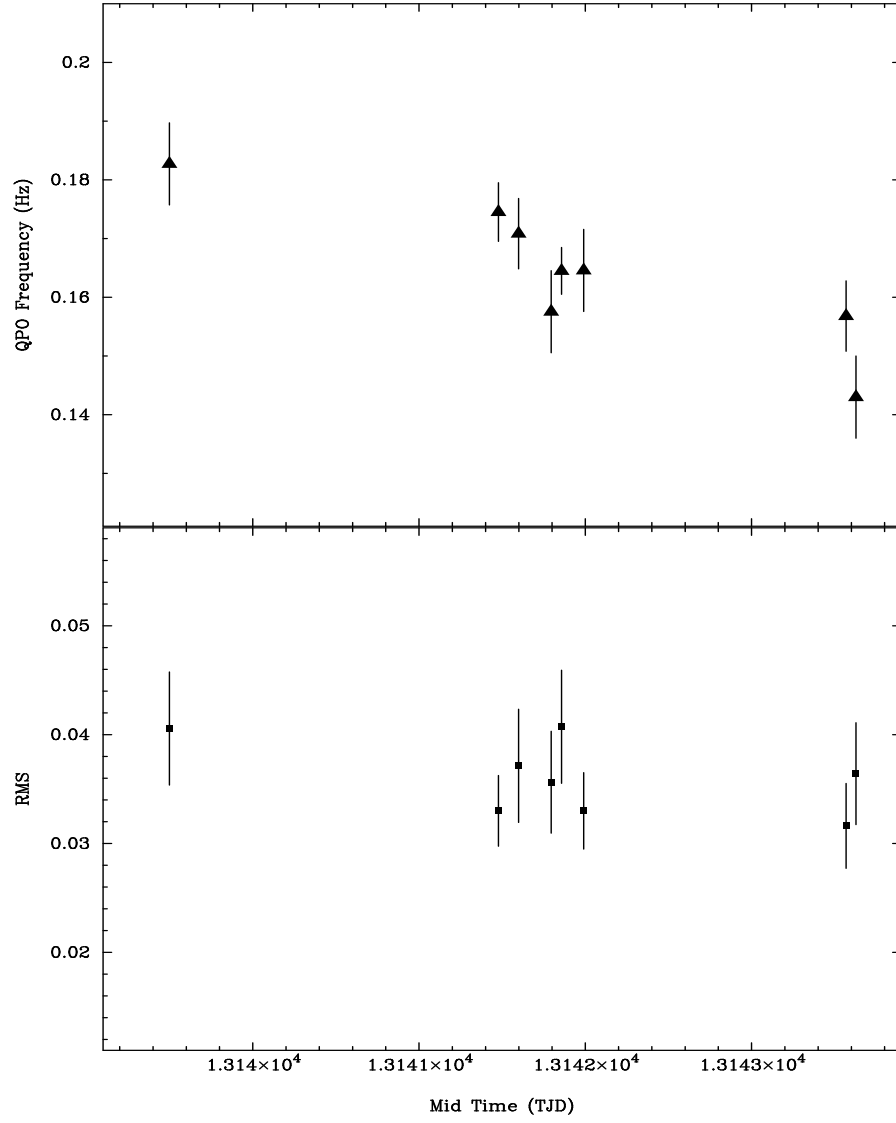


Figure 5. The QPO frequency and the RMS variation in the QPO feature are shown as function of time in the top and the bottom panels respectively.

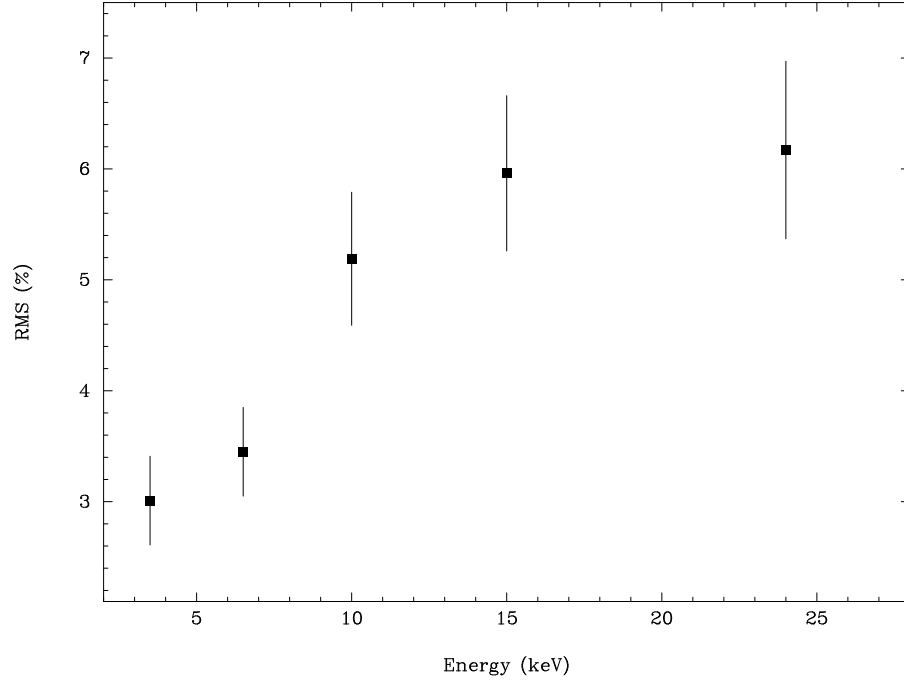


Figure 6. The RMS variation (in percentage) in the QPO feature determined from observation A is shown here as a function of the energy of the X-ray photons.

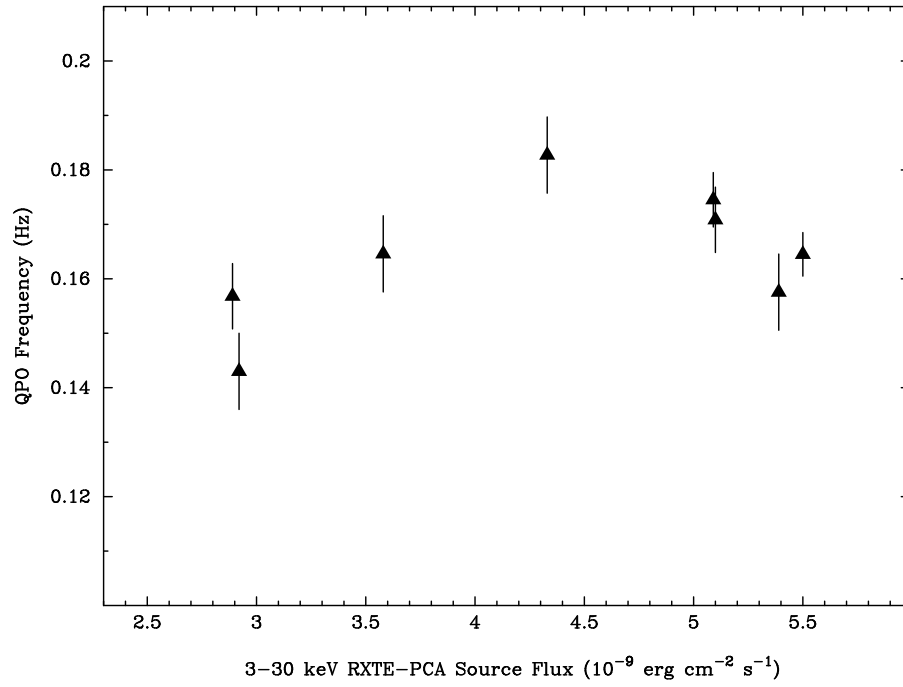


Figure 7. The QPO frequency measured from each segment of the RXTE-PCA light curve are shown here against the 3-30 keV X-ray flux.

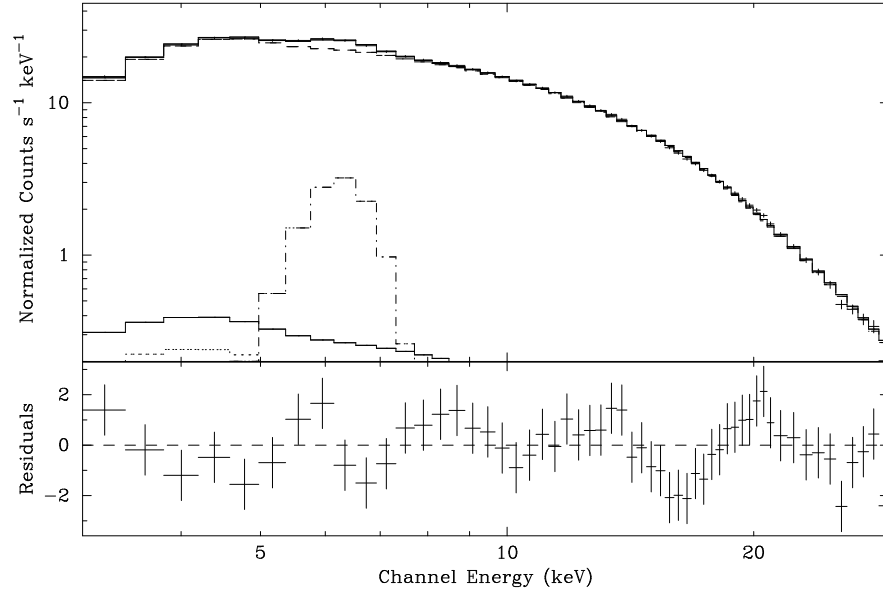


Figure 8. The X-ray spectrum obtained from observation B is shown here along with the best fit model components including a cut-off power law, a Gaussian emission line, and the additive background components as histograms. The residuals to the best fit model are shown in the lower panel in unit of their contribution to the total χ^2 .